

Geophysical Research Letters



RESEARCH LETTER

10.1029/2025GL117448

Key Points:

- Back-projection and dynamic simulations indicate multi-segment rupture of the 1995 M_w 7.2 Nuweiba earthquake
- Supershear rupture can greatly amplify ground shaking, increasing seismic hazard for Gulf of Aqaba coastal communities
- The 1995 Nuweiba event increased fault stress on the Arnona Fault in the southern Gulf of Aqaba, potentially advancing its future rupture

Supporting Information:

Supporting Information may be found in the online version of this article.

Correspondence to:

B. Li, bo.li.3@kaust.edu.sa

Citation:

Li, B., Ulrich, T., Gabriel, A.-A., Suhendi, C., Klinger, Y., Jónsson, S., & Mai, P. M. (2025). Supershear rupture of the 1995 M_w 7.2 multi-segment Nuweiba earthquake in the Gulf of Aqaba. *Geophysical Research Letters*, 52, e2025GL117448. https://doi.org/10.1029/2025GL117448

Received 5 JUN 2025 Accepted 4 NOV 2025

Author Contributions:

Conceptualization: Bo Li, Thomas Ulrich, Yann Klinger, Sigurjón Jónsson, Paul Martin Mai Data curation: Bo Li, Thomas Ulrich, Alice-Agnes Gabriel, Yann Klinger, Sigurjón Jónsson

Formal analysis: Bo Li, Paul Martin Mai Funding acquisition: Alice-Agnes Gabriel, Paul Martin Mai Investigation: Bo Li, Thomas Ulrich, Alice-Agnes Gabriel, Yann Klinger, Sigurjón Jónsson, Paul Martin Mai Methodology: Bo Li, Thomas Ulrich, Alice-Agnes Gabriel, Cahli Suhendi, Yann Klinger, Paul Martin Mai

© 2025. The Author(s).

This is an open access article under the terms of the Creative Commons
Attribution-NonCommercial-NoDerivs
License, which permits use and
distribution in any medium, provided the original work is properly cited, the use is non-commercial and no modifications or adaptations are made.

Supershear Rupture of the 1995 $M_{\rm w}$ 7.2 Multi-Segment Nuweiba Earthquake in the Gulf of Aqaba

Bo Li¹ D, Thomas Ulrich² D, Alice-Agnes Gabriel^{2,3} D, Cahli Suhendi¹ D, Yann Klinger⁴ D, Sigurjón Jónsson¹ D, and Paul Martin Mai¹ D

¹Physical Science and Engineering Division, King Abdullah University of Science and Technology, Thuwal, Saudi Arabia, ²Department of Earth and Environmental Sciences, Ludwig-Maximilians-University München, München, Germany,

Abstract The Gulf of Aqaba (GoA) is the seismically most active region in the Red Sea, with a history of large earthquakes and posing a high seismic hazard to coastal communities. This study uses back-projection and dynamic rupture simulation to investigate the largest instrumentally recorded earthquake in the GoA, the 1995 $M_{\rm w}$ 7.2 Nuweiba earthquake, to understand stress loading, failure mechanisms, and cascading rupture potential on complex multi-segment fault systems. Our results reveal a multi-segment cascading rupture with supershear rupture on the optimally prestressed Aragonese Fault. Supershear rupture significantly amplified offshore ground shaking, elevating seismic hazard for the narrow gulf's coastal regions. This event partially ruptured the GoA fault system, increasing Coulomb stress on the unbroken southern Arnona Fault, which has been silent since 1588. This stress loading likely advanced a future rupture on this critical segment, requiring close monitoring and increased preparedness for a potential large earthquake in the region.

Plain Language Summary The Gulf of Aqaba (GoA) fault system, the seismically most active region in the Red Sea, has hosted multiple large earthquakes in historical times. The rapid development of NEOM, an infrastructural giga-project of the Kingdom of Saudi Arabia, near the GoA highlights the need for seismic hazard assessment (SHA). However, the offshore nature of the fault system and limited data complicate SHA efforts. Studying past earthquakes provides valuable insights into fault loading, failure mechanisms, and rupture, enhancing SHA for the region. In this study, we analyze the rupture process of the magnitude 7.2 1995 Nuweiba earthquake, the largest instrumentally recorded earthquake in the GoA. Our findings reveal a multi-segment cascading rupture, including a supershear rupture on the central Aragonese Fault. Supershear ruptures amplify seismic hazard in this narrow gulf region, with intensified and prolonged ground shaking, posing a severe threat to coastal communities in the event of future earthquakes. The 1995 event only partially ruptured the GoA fault system, increasing stress on the Arnona Fault, which has not ruptured since 1588. This stress loading could advance a future earthquake on this critical segment, highlighting the need for close monitoring and strengthened preparedness to mitigate potential earthquake risk in the region.

1. Introduction

The Gulf of Aqaba (GoA) constitutes a ~180 km long southern section of the Dead Sea Transform Fault (DSTF). This left-lateral strike-slip plate boundary separates the Arabian plate from the Sinai micro-plate (Ben-Avraham et al., 1979; Eyal et al., 1981). South of the gulf, the fault system connects with the Red Sea mid-ocean ridge. The GoA consists of three primary strike-slip segments: the Eilat Fault (EF) in the north, the Aragonese Fault (AF) in the center, and the Arnona Fault (ArF) in the south, forming an en echelon strike-slip fault system (Barjous & Mikbel, 1990) (Figure 1). These segments are separated by pull-apart basins bounded by stepover normal faults dipping toward the basins (Ben-Avraham, 1985; Daggett et al., 1986). Additionally, the region features several coastal normal faults, including the Haql Fault (HF), Dakar Fault (DF), and Tiran Fault (TF). Together with several secondary fault branches, these faults form the intricate and geometrically complex GoA fault system (Ribot et al., 2021).

The GoA fault system has been the seismically most active segment of the DSTF over the last century and the seismically most active region in the Red Sea (Elhadidy et al., 2021; Mogren, 2021). Notably, it hosted the widely felt and locally damaging Nuweiba earthquake on 22 November 1995, with a reported magnitude of approximately M 7.2 (referred to hereafter as $M_{\rm w}$ 7.2). This event remains the largest instrumentally recorded seismic

LI ET AL.

³Scripps Institution of Oceanography, UC San Diego, La Jolla, CA, USA, ⁴University Paris Cité, Institut de Physique du globe de Paris, CNRS, Paris, France

onlinelibrary.wiley.com/doi/10.1029/2025GL117448 by Cochrane France, Wiley Online Library on [17/11/2025]. See the Terms and Condition

Project administration: Bo Li, Alice-Agnes Gabriel, Paul Martin Mai Resources: Bo Li, Alice-Agnes Gabriel, Yann Klinger, Sigurjón Jónsson Software: Bo Li, Thomas Ulrich, Alice-Agnes Gabriel, Cahli Suhendi Supervision: Bo Li, Alice-Agnes Gabriel, Yann Klinger, Sigurjón Jónsson, Paul Martin Mai

Validation: Bo Li, Thomas Ulrich, Alice-Agnes Gabriel, Yann Klinger, Sigurjón Jónsson, Paul Martin Mai Visualization: Bo Li, Thomas Ulrich, Cahli Suhendi, Yann Klinger, Sigurjón Jónsson, Paul Martin Mai Writing – original draft: Bo Li, Paul Martin Mai

Writing – review & editing: Bo Li, Thomas Ulrich, Alice-Agnes Gabriel, Yann Klinger, Sigurjón Jónsson, Paul Martin Mai

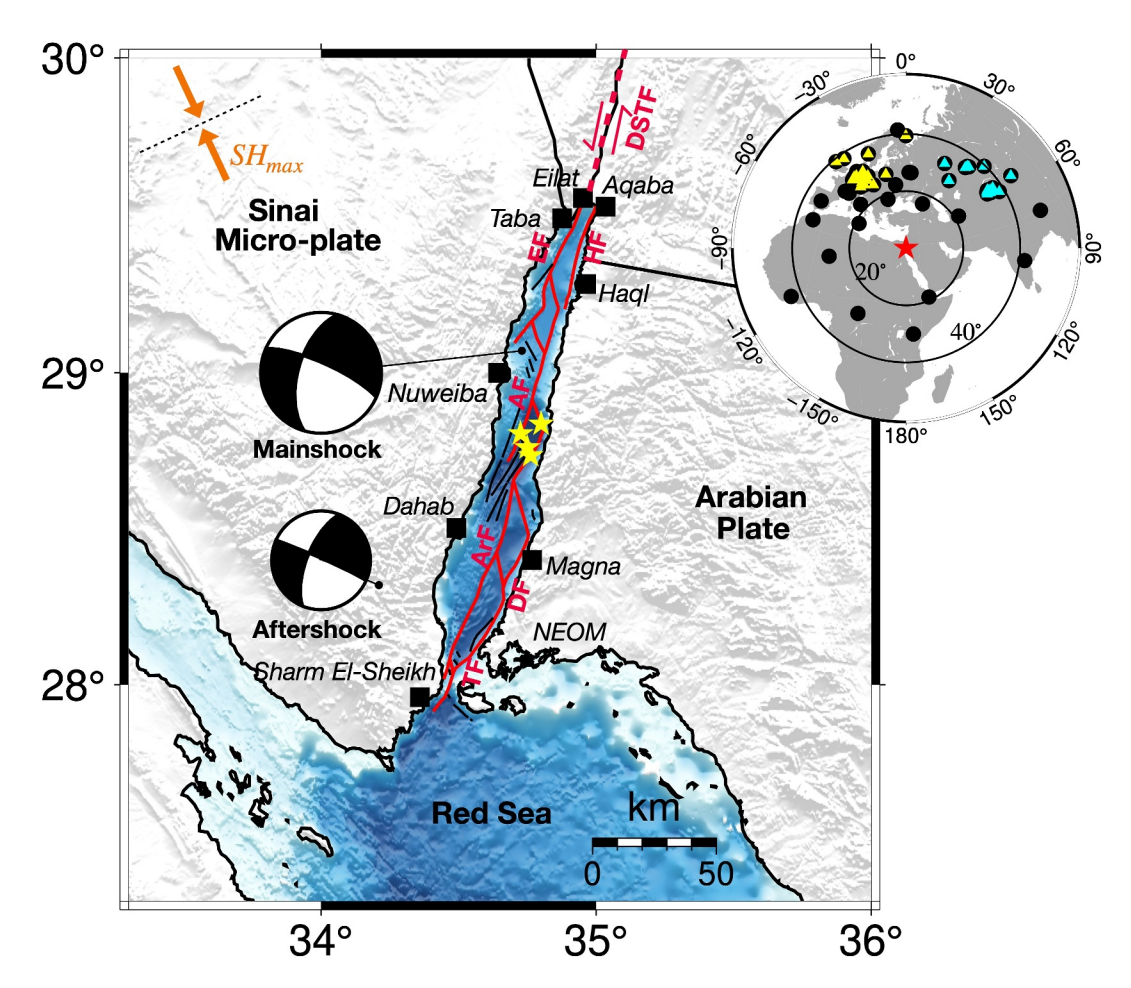


Figure 1. Map of the Gulf of Aqaba and its fault system. The "beach balls" represent the moment tensor solutions for the 1995 $M_{\rm w}$ 7.2 Nuweiba earthquake and a selected aftershock ($M_{\rm w}$ 5.3, 22 November 1995), from the Global Centroid Moment Tensor (GCMT) database. The four yellow stars mark the potential epicenters of the earthquake used in back-projection. Black lines in the Gulf represent branch fault segments, while red lines show the modified fault traces used for dynamic modeling, both based on Ribot et al. (2021). Abbreviations: EF—Eilat Fault; AF—Aragonese Fault; ArF—Arnona Fault; HF—Haql Fault; DF—Dakar Fault; TF—Tiran Fault; DSTF—Dead Sea Transform Fault. The orange arrows in the top left denotes the orientation of the maximum horizontal compressive stress. The top right inset shows teleseismic arrays used in the back-projection and supershear Rayleigh wave analysis. Yellow and cyan triangles indicate stations from the European Array and Asian Array, respectively, used for the back-projection. Stations used for the supershear Rayleigh wave analysis are shown as black solid circles. The two unfilled black circles represent distances of 20° and 40° from the epicenter of the $M_{\rm w}$ 7.2 Nuweiba earthquake.

event on the DSTF and in the Red Sea. It primarily ruptured the northern section of the GoA fault system (Hofstetter, 2003; Klinger et al., 1999).

Historical earthquakes, inferred from seismo-turbidite analysis of sediment cores, suggest that at least two past events, in 1068 and 1588, ruptured the entire Gulf of Aqaba fault system (Bektaş et al., 2024). These findings align with probabilistic seismic hazard assessment (PSHA) indicating there is a potential for large earthquakes of up to $M_{\rm w}$ 7.6 in the region (Al-shijbi et al., 2019; Elhadidy et al., 2021). With its capacity to generate $M_{\rm w}$ 7.2 or larger earthquakes, the GoA fault system poses a significant seismic hazard to rapidly developing areas like NEOM and nearby coastal communities. However, the offshore nature of the fault system and limited data availability present considerable challenges for reliable seismic hazard assessment (SHA).

Detailed analysis of large (M > 7) earthquakes that occurred in the past decades can provide valuable insights into fault loading, failure criteria, and the potential for cascading ruptures within multi-segment fault networks, thereby enhancing regional seismic hazard assessment (Kaneko et al., 2010; Klinger et al., 2018; B. Li et al., 2023; Taufiqurrahman et al., 2023). Despite being the largest instrumentally recorded earthquake in the Gulf of Aqaba, the limited local and regional data make it difficult to accurately pinpoint the initiation location and to identify the

LI ET AL. 2 of 13

fault segments that ruptured during the 1995 $M_{\rm w}$ 7.2 Nuweiba event. Previous studies indicate that the main rupture of the 1995 Nuweiba earthquake occurred close to the Aragonese Deep (Baer et al., 2008; Hofstetter et al., 2003; Klinger et al., 1999; Pinar & Türkelli, 1997). However, exact location of epicenters vary. Using teleseismic waveforms, some studies suggest dominant normal faulting for the first subevent, indicating that the rupture initiated on the stepover normal fault between the Aragonese and Arnona faults (Abdel-Fattah et al., 2006; Pinar & Türkelli, 1997). In contrast, Klinger et al. (1999) suggest that the first subevent occurred on the eastern side of the Aragonese Deep, aligning with the northern segment of the strike-slip Arnona Fault. This interpretation is consistent with recent Bayesian inversions that integrate both geodetic and teleseismic data (Vasyura-Bathke et al., 2024). Additionally, it remains uncertain whether the 1995 Nuweiba earthquake terminated on a normal fault or a strike-slip fault in the northern gulf.

With advancements in high-performance computing, dynamic rupture modeling has become a critical tool for physics-based ground-motion simulations that may inform seismic hazard assessment (Galvez et al., 2020; B. Li et al., 2023; Mai et al., 2018; Wirp et al., 2024; Xin & Zhang, 2021). Its capability to incorporate 3D Earth structure, including topography and bathymetry, 3D seismic-wave propagation, complex fault geometry with fault roughness, and rupture dynamics with potential off-fault plasticity significantly enhances our understanding of ground motion properties. Ensemble simulations can also account for uncertainties in fault models, prestress loading, and frictional properties, enabling the simulation of alternative mechanically plausible rupture scenarios and their resultant ground motions (B. Li et al., 2023), thereby providing deeper insights and serves as a valuable complement to seismic hazard assessment.

In this study, we first apply back-projection to obtain a first-order understanding of the rupture process of the 1995 Nuweiba earthquake and identify the fault segments potentially involved. The back-projection results suggest the possibility of a supershear rupture during the event. Next, we examine the resemblance of Rayleigh waves between the 1995 Nuweiba earthquake and a collocated aftershock with a similar focal mechanism to further investigate the presence of supershear rupture. Building on these findings, we develop three plausible rupture scenarios that account for uncertainties and use the open-source code SeisSol to perform fully 3-D spontaneous dynamic rupture simulations of the 1995 Nuweiba event. Finally, we evaluate the resulting ground shaking and assess the event's implications for future seismic activity along the Gulf of Aqaba fault system.

2. Back-Projection and Supershear Rupture

2.1. Back-Projection

We analyze the coseismic rupture process using the back-projection approach with global seismic arrays. Back-projection utilizes the time-reversal property of curved wavefronts recorded by seismic arrays to image the spatiotemporal evolution of high-frequency seismic radiation in sliding time windows (Ishii et al., 2005; Krüger & Ohrnberger, 2005). With its computational efficiency and minimal prior knowledge requirements—primarily an assumed velocity model and a rough estimate of the rupture area—back-projection has become a routine method for rapidly tracking the rupture process of large and moderate earthquakes (Ishii et al., 2007; B. Li & Ghosh, 2017; Mai et al., 2023; Zhang et al., 2023).

Assuming sub-vertical fault segments within the Gulf of Aqaba fault system, we perform back-projection constrained to the mapped fault traces. We fix the source depth at 10 km considering the poor depth resolutions of back-projection (Ishii et al., 2005; B. Li et al., 2024) and shallow locking depth of faults in Gulf of Aqaba (X. Li et al., 2021; Castro-Perdomo et al., 2022). Cross-correlation (CC) of first-arrival P-waves is commonly employed to correct waveform polarity and estimate travel-time biases using a 1D velocity model. However, this requires knowledge of the hypocenter location, which has not been well determined for this event. Therefore, we perform four realizations of back-projection, each based on a potential hypocenter on a different fault segment (Figure 1), to account for varying rupture nucleation hypotheses proposed in previous finite-fault inversions (Baer et al., 2008; Hofstetter et al., 2003; Shamir et al., 2003; Vasyura-Bathke et al., 2024). We utilize two global teleseismic arrays: the European array and Asian Array (Figure 1). For each array, we estimate travel-time biases relative to the hypothesized hypocenter by applying a cross-correlation method to a 10-s window around the direct P-wave phase within a frequency range of 0.25–1 Hz. Only stations with an average correlation coefficient $CC \ge 0.65$ are included in the back-projection analysis. Then we employ a 4-s sliding time window with a 0.1-s time step across the continuous data, including the event signals, to image the rupture process.

LI ET AL. 3 of 13

19448007, 2025, 22, Downlo.

aded from https://agupubs.onlinelibrary.wiley.com/doi/10.1029/2025GL117448 by Cochrane France, Wiley Online Library on [17/11/2025]. See the Terms and Co

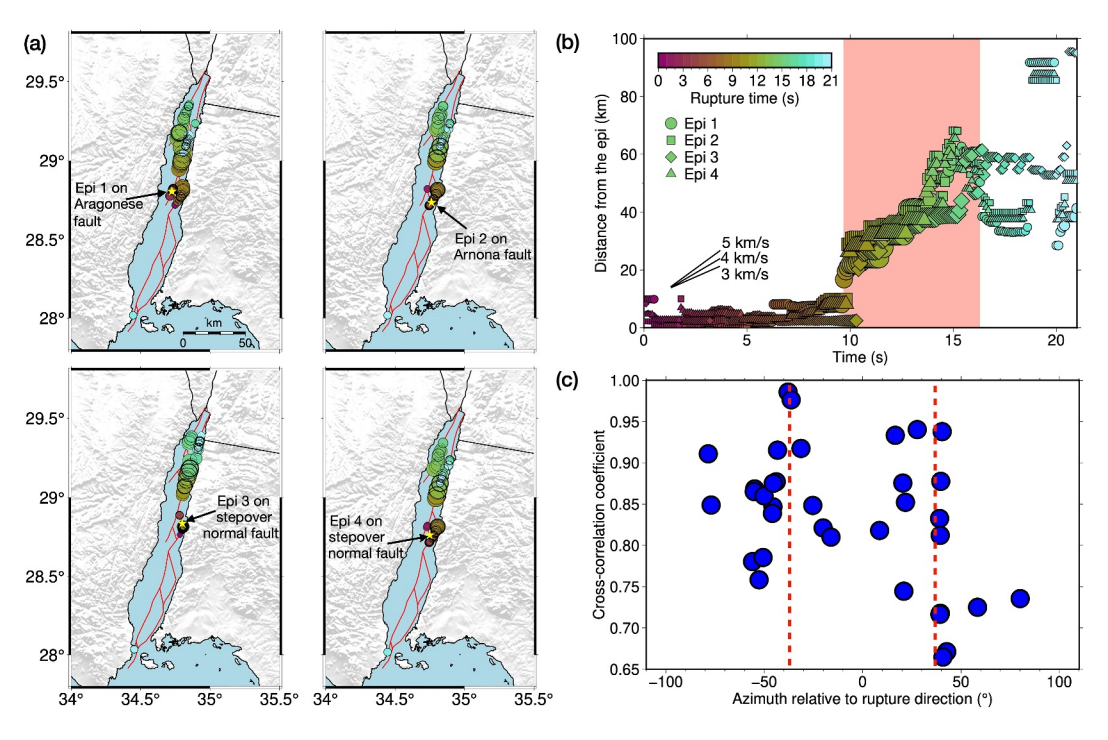


Figure 2. The rupture process for the $M_{\rm w}7.2$ Nuweiba earthquake imaged by the back-projection and supershear rupture evidence. (a) Back-projection results from the European array, with each panel corresponding to a hypothesized epicenter location (Epi, yellow star). (b) Evolution of rupture distance over time relative to the hypothesized initiation location. The pink-shaded region highlights a relatively faster rupture velocity on the Aragonese Fault. (c) Rayleigh waveform cross-correlation between the mainshock and a collocated aftershock with a similar focal mechanism, as shown in Figure 1. The two red dashed lines indicate $\pm 38^{\circ}$ relative to the rupture direction.

Back-projection results of both arrays consistently show that the initial rupture phase occurred on the northern Arnona Fault (ArF), regardless of the assumed hypocenter location (Figure 2a; Figure S1a in Supporting Information S1). This finding aligns with the inversion models presented by Klinger et al. (1999) and Vasyura-Bathke et al. (2024). If the assumed hypocenters were located elsewhere, the imaged rupture rapidly propagates to and is subsequently imaged on the Arnona Fault. The results also illustrate a multi-segment rupture involving the Arnona Fault and Aragonese Fault, and the stepover normal faults in between. In addition, a notably higher rupture velocity, with average value $V_r \ge 4$ km/s on the northern Aragonese Fault, is consistently observed across both arrays (Figure 2b; Figure S1b in Supporting Information S1). This velocity exceeds the shear-wave velocity depicted in the 1D velocity model (Tang et al., 2016) (Figure S2 in Supporting Information S1), suggesting the occurrence of a supershear rupture during this event.

As the rupture propagates farther from the hypocentral region, the uniformly applied time-bias calibration based on the hypothesized hypocenter becomes less valid. In addition, interference from depth phases further contributes to increased location uncertainties. These factors lead to notable uncertainty regarding the ruptured northern segments, particularly whether the rupture extended along the Eilat Fault or the nearby coastal Haql Fault (Figure 2; Figure S1 in Supporting Information S1).

2.2. Supershear Validation

The back-projection results indicate a potential supershear rupture along the Aragonese Fault. To further investigate the existence of a supershear rupture, we check the waveform similarity between the mainshock and a smaller collocated aftershock ($M_{\rm w}$ 5.3) with a similar focal mechanism (Figure 1). Previous studies suggest that within the Rayleigh wave Mach-cone zone, the waveforms between the mainshock and aftershock should closely resemble each other at periods shorter than the supershear event's rupture duration but longer than its rise time, while the similarities decrease when moving outside of the Mach-cone zone (Bao et al., 2019; Vallée & Dunham, 2012). We compare the Rayleigh wave similarity in the period range between 15 and 20 s (Figure S3 in Supporting Information S1) for stations within an epicentral distance of 15°-45° (black circles in Figure 1). The

LI ET AL. 4 of 13

results in Figure 2c reveal the highest cross-correlation coefficient (up to 0.99) within a narrow zone around 38° (relative to the northward rupture direction on the Aragonese Fault, θ), but much lower correlation coefficient in other directions. Assuming a Rayleigh wave velocity (V_R) of 3 km/s (Corchete et al., 2007), the rupture velocity (V_r) is calculated as $V_R/\cos(\theta) = 3/\cos(38^\circ) = 3.8$ km/s, exceeding the S-wave velocity at depths shallower than 20 km (Figure S2 in Supporting Information S1), thereby confirming the supershear rupture process. Furthermore, the supershear rupture section coincides with a noticeable reduction in aftershock activity (Klinger et al., 1999), consistent with previous observations of supershear earthquakes (Bouchon & Karabulut, 2008; Wen et al., 2009).

3. Dynamic Rupture Modeling

3.1. Fault Model

We construct the fault model based on the recent fault trace mapping from high-resolution multi-beam imaging of the Gulf of Aqaba (Ribot et al., 2021), where 41 fault segments have been identified. Building on this mapping, as well as insights from previous fault inversion studies and the back-projection results of our analysis, we select the primary strike-slip segments, the connecting normal stepover segments, and the major coastal normal faults to define the fault model for simulating the 1995 Nuweiba earthquake (red lines in Figure 1). Additionally, through a series of tests, we introduce model modifications by connecting the strike-slip faults with the stepover normal faults (Figure 1), enabling rupture cascading across segments.

In our fault model, the strike-slip segments are set to be vertical, the coastal normal faults are assigned a dip of 80° to the west, and the stepover normal faults are given a dip of 70° toward their associated pull-apart basin. As a transitional zone between Red Sea spreading and Dead Sea transform motion, the Gulf of Aqaba exhibits crustal thinning, as inferred from geophysical and geodetic studies (Abdelazim et al., 2023; Castro-Perdomo et al., 2022; Ginzburg et al., 1981; Hamouda et al., 2019). To account for this, we limit the rupture extent at depth by smoothly tapering deviatoric stresses between 12 and 16 km, aligning with the 13 km locking depth estimated in the GPS study by Mahmoud et al. (2005). At the surface, the non-planar faults intersect with the complex topography and bathymetry, sampled at a resolution of ~122 m. Additionally, we incorporate fault roughness on the fault planes, modeled with a self-similar fractal distribution (Power & Tullis, 1991) over length scales from 100 m up to the fault dimensions, with a maximum cutoff at 50 km. Following Fang and Dunham (2013), the amplitude-to-wavelength ratio of natural faults ranges from 10^{-3} to 10^{-2} ; in our model, we adopt a ratio of $10^{-2.7}$. The same random seed is applied across all fault segments.

The fault model is embedded in a 1D velocity structure (Castro-Perdomo et al., 2022; Tang et al., 2016). We follow the approach outlined by Ulrich, Gabriel, et al. (2019) to constrain the initial fault stress and strength, and assume a non-associated Drucker-Prager elasto-viscoplasticity rheology to model coseismic off-fault energy dissipation (Wollherr et al., 2018, 2019). Further details are provided in Text S1 in Supporting Information S1: Dynamic Model Parameterization. We use the open-source software SeisSol to run 3D dynamic rupture and seismic wave propagation simulations; subsequently, we analyze the resulting ground-motion properties as well as the Coulomb stress changes on the surrounding fault segments.

3.2. Rupture Dynamics and Synthetics

The resolution of back-projection using limited array data cannot well constrain the northern rupture of the 1995 Nuweiba earthquake, leaving ambiguity about whether it propagated along the Eilat Fault or the coastal Haql Fault (HF), which are approximately 10 km apart. Additionally, depth phases, coda waves, and the heterogeneous velocity structure—distinct from the nucleation region—further complicate the identification of the rupture pathway. Under the proposed regional stress field, an evaluation of prestress loading reveals that the strike-slip segments are more optimally oriented and dynamically favored for rupture compared to the coastal normal faults, despite their similar fault trends (Figure S4 in Supporting Information S1).

With these constraints and assumptions, we develop a preferred dynamic rupture model. The rupture is artificially nucleated in the northern section of the Arnona Fault and propagates bilaterally (Figure 3a). To the south, the rupture quickly terminates at a geometric complexity, where changes in fault orientation modulate the prestress loading, increasing resistance to rupture (Figure S4 in Supporting Information S1). Meanwhile, the rupture breaks the stepover normal faults simultaneously and subsequently triggers rupture on the Aragonese Fault. This

LI ET AL. 5 of 13

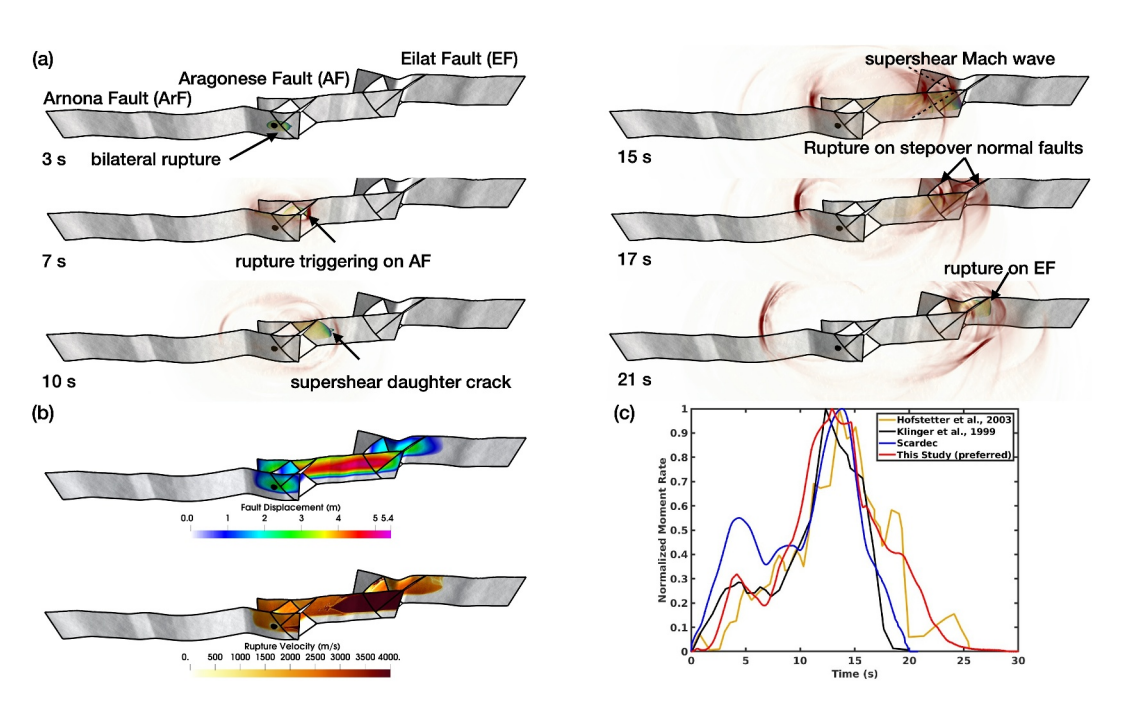


Figure 3. A dynamic rupture scenario for the 1995 $M_{\rm w}$ 7.2 Nuweiba earthquake. (a) Snapshots of the absolute slip rate and surface seismic wavefield, highlighting the complex rupture process for the earthquake, at rupture times of 3, 7, 10, 15, 17, and 21 s. The labels indicate noteworthy features of the rupture. Black circles represent the hypocenter location on the ArF. The unruptured coastal faults are omitted from this figure to provide clearer visualization of the rupture dynamics. (b) Final rupture velocity and fault displacement of the simulation. (c) Comparison of normalized moment rate functions (MRFs), with the SCARDEC MRF taken from Vallée et al. (2011), and the MRF inferred by Klinger et al. (1999) and Hofstetter et al. (2003).

correlates with the first peak in the moment rate function (MRF) (Figure 3c). While the northward rupture on the Aragonese Fault is directly triggered, there is a short delay for the southward (or backward) rupture on Aragonese Fault. This delay is attributed to asymmetrical and progressively increasing stress changes induced by accumulating slip along the intersected stepover normal faults on either side of the Aragonese Fault, a phenomenon similar to the rupture delay also observed during the 2023 $M_{\rm w}$ 7.8 Türkiye earthquake (Gabriel et al., 2023; B. Li et al., 2025). The combined influence of dynamic stress effects and optimal prestress loading causes the northward rupture on the Aragonese Fault from subshear to supershear, accompanied by a daughter crack and a Mach-wave cone (Figure 3a and Movie S1). Together with the bilateral rupture, this northward supershear transition contributes to the second and largest peak in the moment rate function (Figure 3c). The supershear rupture section of the Aragonese Fault coincides with a large slip asperity, exhibiting a maximum slip of up to 5.4 m on the Aragonese Fault (Figure 3b). Following this, the northward rupture continues, sequentially triggering the stepover normal faults that connect with the Eilat Fault. Slip on the stepover normal faults dynamically affects the Aragonese Fault, producing a distinct slip pattern characterized by much lower slip amplitude north of the intersection (Figure 3b). The rupture then smoothly terminates on the Eilat Fault at around 25 s, where a prescribed gradual reduction in prestress is applied. Without this stress constraint, the rupture would propagate through the entire fault, which is inconsistent with observed surface displacement data and aftershock distributions that do not extend to the end of this segment (Hofstetter, 2003; Klinger et al., 1999; Shamir et al., 2003; Vasyura-Bathke et al., 2024). This scenario produces an $M_{\rm w}$ 7.27 rupture.

To further investigate the initial rupture phase and complement the back-projection analysis, we conducted dynamic simulations with scenarios nucleating on the southern section of the Aragonese Fault (AF) and the stepover normal fault connecting the AF and ArF (Figure S5 in Supporting Information S1). While all scenarios yield a broadly similar fault displacement distribution on the commonly ruptured AF and Eilat Fault (EF) (Figure S5a in Supporting Information S1), they exhibit distinct differences in the details of their moment rate functions (Figure S5b in Supporting Information S1). The results indicate that nucleation on the southern AF also produces a two-peak moment rate function. However, the first peak is relatively higher, and the second peak is notably

LI ET AL. 6 of 13

narrower compared to previous kinematic studies. In contrast, nucleation on the stepover normal fault does not distinctly capture the imprint of the first "sub-event," and the peak moment rate release occurs a few seconds earlier. Furthermore, both alternative scenarios failed to trigger rupture on the northern ArF, particularly the scenario with nucleation on the southern AF. The initial left-lateral slip on the southern section of the AF, combined with the acute angle between the AF and the stepover normal faults, do not favor backward branching rupture propagation (Fliss et al., 2005). Additionally, the acute angle between the stepover normal faults and the ArF further impedes northward rupture propagation along the ArF. Furthermore, a sustained subshear rupture scenario with the same nucleation location as the preferred model produces three peaks in the MRF and a longer rupture duration than previous kinematic inversions, resulting in a poorer match compared to the preferred supershear scenario (Figure S5 in Supporting Information S1).

The simulation results of the preferred multi-segment rupture are consistent with previous studies and observations of the 1995 Nuweiba earthquake. The two-crest moment rate function (MRF) closely aligns with MRFs derived from published kinematic fault inversion studies (Hofstetter et al., 2003; Klinger et al., 1999; Vallée et al., 2011). For comparison of teleseismic waveforms, we discretize the rupture into 90 point sources (30 along strike and 3 along dip) to adequately capture the source properties and ensure reliable synthetic waveform generation. The moment tensor for each point source is calculated by averaging the moment tensors of fault element faces in the ruptured subregion (Ulrich et al., 2022). Synthetic teleseismic waveforms are then generated using precomputed Green's Functions (see Data Availability Statement for details). These low frequency teleseismic waveforms, though not highly sensitive to the details of the rupture process, exhibit a good match with surface waveform observations from teleseismic stations across all azimuths (Figures S6 and S7 in Supporting Information S1), reproducing both phase arrivals and amplitude characteristics.

4. Discussion

The offshore rupture and limited local and regional data complicate the precise determination of the rupture initiation point and the fault segments involved in the 1995 Nuweiba earthquake. Uncertainties in the hypocenter locations also limit the direct application of back-projection with travel time corrections for imaging the coseismic rupture process, especially the initial rupture phase. However, by assuming and testing all highly plausible hypocenter locations across different segments, back-projection effectively demonstrates its capability to identify the most likely rupture scenario. Both back-projection analysis and dynamic rupture simulations with various hypocenter locations on different fault segments consistently indicate that the rupture initiated on the northern Arnona Fault (ArF) and then triggered multi-segment rupture. This nucleation around the intersection of strike-slip and stepover normal faults reconciles inconsistencies in the reported nucleation phase among previous studies (Baer et al., 2008; Hofstetter et al., 2003; Klinger et al., 1999; Pinar & Türkelli, 1997; Vasyura-Bathke et al., 2024). The 1995 Nuweiba earthquake appears to have simultaneously broken both the northern segment of the strike-slip ArF and the stepover normal faults that connecting with the AF at the onset of the event, generating a very complex radiation pattern.

Compared to the well-constrained initial rupture process revealed by back-projection, the termination phase of the 1995 Nuweiba earthquake remains poorly constrained and hence uncertain. Back-projection results from different arrays suggest that the rupture most likely terminated on the Eilat Fault (EF). However, due to the limited resolution of the back-projection, some interpretations also allow for the possibility of termination on the Hagl Fault (HF) near the eastern coast (Figure 2; Figure S1 in Supporting Information S1). In this study, we select termination on the EF as the preferred model, given its more favorable prestress loading (Figure S4 in Supporting Information S1). However, this assessment is based on the assumption of a uniform regional stress field for both EF and HF. Recent studies indicate that non-uniform stress fields, with significant stress rotations, may be present within the same fault network. For instance, a regional stress rotating along the East Anatolian Fault (Güvercin et al., 2022; Yilmaz et al., 2006) and the Sürgü-Misis Fault (Koc & Kaymakcı, 2013) leads to the 2023 $M_{\rm w}$ 7.8 and M_w 7.6 Türkiye Kahramanmaraş earthquake doublet (Gabriel et al., 2023; B. Li et al., 2025). Tectonic studies in the Gulf of Aqaba show evidence of plate rotation, further supporting the complex regional stress field (Bosworth et al., 2019; Lyberis, 1988). This non-uniform stress regime, combined with the stress loading from historical earthquakes, likely results in a more complex prestress distribution across the fault system (Kaneko et al., 2010; Taufiqurrahman et al., 2023). Such a configuration may bring coastal normal faults closer to failure, potentially triggering them to rupture in conjunction with the strike-slip segments, thereby potentially increasing seismic hazard for coastal communities.

LI ET AL. 7 of 13

In addition to uncertainties in the regional stress conditions, the offshore fault system and limited data availability introduce ambiguity in frictional properties and fault geometry, including the connectivity of fault segments, seismogenic depth, dip angles, and roughness levels (Fang & Dunham, 2013; B. Li et al., 2023). However, all alternative fault models should be able to reproduce the 1995 $M_{\rm w}$ 7.2 Nuweiba earthquake, capturing the observed rupture cascading, overall rupture extent, and key dynamic features, comparable to those of the preferred model presented in this study, while remaining viable for a full rupture cascade across the entire fault network to be consistent with the record of historic earthquakes (Bektas et al., 2024).

A reduced prestress was applied on the Eilat Fault to inhibit rupture from propagating along its entire length, consistent with observed surface displacements and aftershock distributions (Klinger et al., 1999). This heterogeneous prestress may be due to previous local earthquake activity on the Eilat Fault. Seismo-turbidite records from Bektaş et al. (2024) show a localized turbidite near the termination, which could be attributed either to a localized flooding event or an earthquake. Alternatively, a western branch fault connecting to the Eilat Fault (Figure 1) may have modified the prestress loading, with left-lateral slip producing heterogeneous stress on both sides of the intersection. In addition, variations in local geological setting, such as sedimentary layers or velocity structure, could also contribute to rupture termination. A comparable case occurred in the 2025 $M_{\rm w}$ 7.7 Myanmar earthquake, where rupture termination on a simple fault coincided with a transition from post-Pliocene alluvial fans to the volcanic Singu basalt unit (Choi et al., 2018; Mai et al., 2025).

The potential for supershear rupture within the GoA fault system increases the seismic hazard for coastal communities along the narrow Gulf of Aqaba. Subshear rupture tends to produce strongly focused energy radiation, generating intense shaking primarily in the near-fault region and in the rupture's forward direction (Andrews, 2010). In contrast, supershear rupture concentrates energy within the Mach cone, resulting in elevated and sustained ground-motion intensity over greater distances but confined to the Mach zones (Dunham & Bhat, 2008). The coherence of Mach waves can be disrupted by rupture and medium heterogeneities, thereby diminishing their amplification effect (Vyas et al., 2018). Figure 4a shows the peak ground velocity (PGV) distribution for the preferred rupture scenario of the 1995 Nuweiba earthquake. To the south, strong directivity amplification is evident from the subshear rupture on the Aragonese Fault, whereas to the north, the transition to supershear mitigates the directivity effect but produces intensified shaking in the off-fault coastal areas within the Mach zones.

These characteristics of subshear and supershear rupture are not unique to the GoA fault system. Similar behaviors have been observed along other major strike-slip faults worldwide, including the 2018 $M_{\rm w}$ 7.5 Palu earthquake on the Palu-Koro Fault, the 2023 $M_{\rm w}$ 7.6 Türkiye earthquake on the Sürgü-Misis Fault, and the 2025 $M_{\rm w}$ 7.7 Myanmar earthquake on the Sagaing Fault (Ulrich, Vater, et al., 2019; B. Li et al., 2025; Mai et al., 2025). The widespread occurrence of supershear rupture and off-fault Mach-zone amplification highlights the importance of considering supershear scenarios in regional seismic hazard assessment for other strike-slip faults, such as the San Andreas Fault.

The 1995 Nuweiba earthquake resulted in positive Coulomb failure stress changes (ΔCFS) on the southern Haql and Arnona faults (Figure 4b), advancing these segments closer to failure. The potential rupture of the Arnona Fault in particular increases the seismic hazard to the NEOM region. Seismo-turbidite records suggest that the most recent large earthquake in the southern Gulf of Aqaba occurred in 1839, likely rupturing only part of the Tiran or Arnona Faults, or one of the secondary faults in the southern gulf (Bektaş et al., 2024). Beyond this, most of the Tiran and Arnona Faults have remained unruptured since the 1588 event.

The post-rupture on-fault Coulomb failure stress change (ΔCFS) transmitted from the ruptured segments in the 1995 Nuweiba earthquake to the unbroken segment show a positive $\Delta CFS \geq 1$ MPa south of the southern rupture edge on the Arnona Faults (Figure 4b). This segment is optimally oriented relative to the regional stress field (Figure S4 in Supporting Information S1) and may already be highly prestressed. As a result, the 1995 Nuweiba earthquake likely advanced the time of occurrence of a future rupture on this segment. Previous studies suggest that geometrical complexities can act as preferred nucleation sites due to stress concentrations from prior earthquakes (Duan & Oglesby, 2005, 2007), indicating that nucleation on the northern Arnona Fault, just south of the complex geometry where the 1995 rupture terminated, may be plausible. The optimally prestressed linear segment is also favorable for supershear rupture, potentially leading to intensified ground shaking in the rapidly developing NEOM area. This highlights the need for close monitoring and strengthened preparedness to mitigate potential seismic hazards in the region.

LI ET AL. 8 of 13

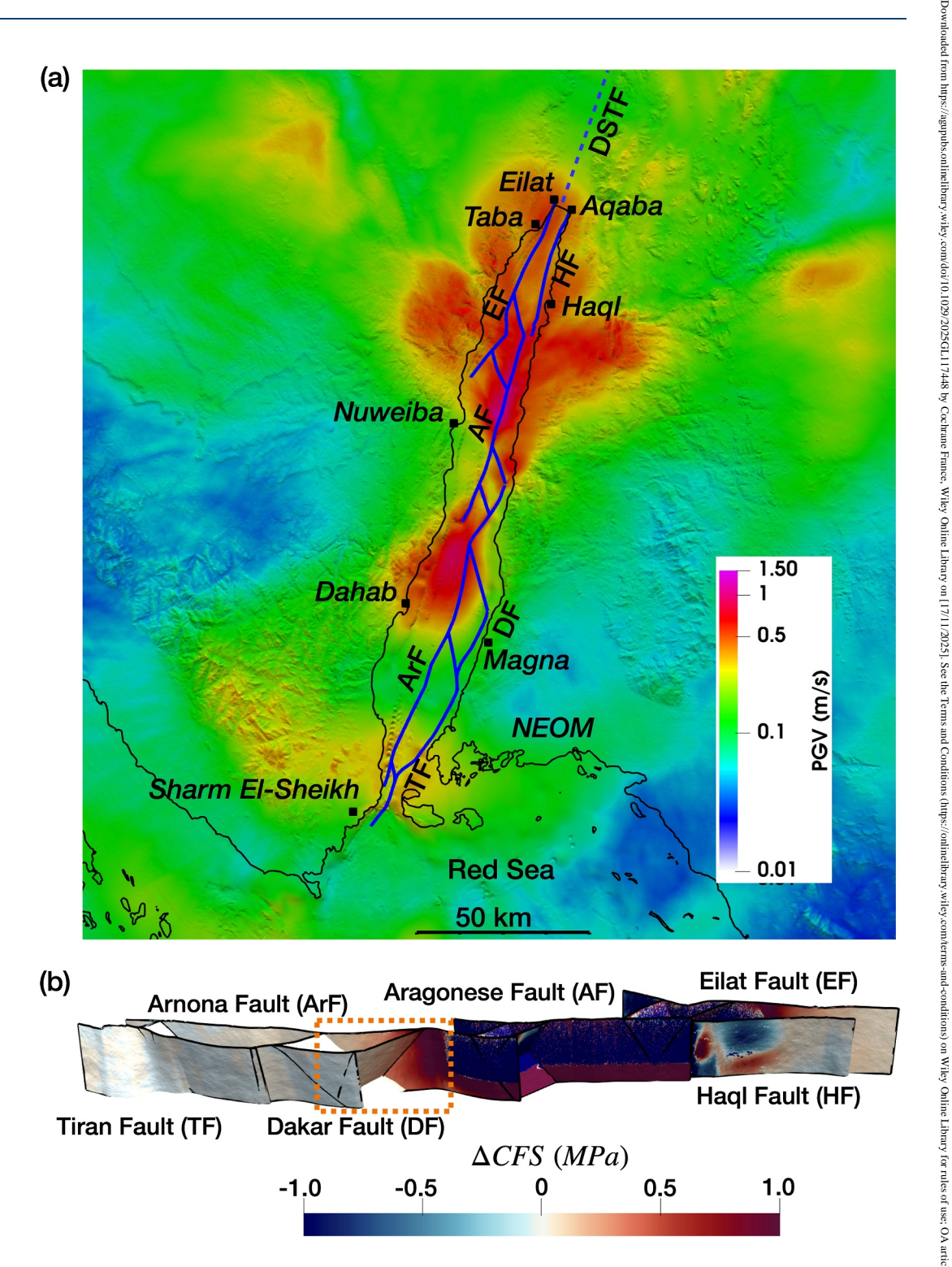


Figure 4. Computed ground shaking and the Coulomb failure stress change (ΔCFS) from dynamic rupture simulations of the 1995 Nuweiba earthquake. (a) Physics-based ground motion simulations showing peak ground velocity (PGV) in m/s for the synthetic Nuweiba event. The black squares denote the major cities in the region. (b) Postseismic Coulomb failure stress change (ΔCFS) resulting from the 1995 Nuweiba earthquake. The scattering observed within the ruptured segments reflects the roughness and heterogeneous slip on the fault plane. The color bar is saturated at ± 1 MPa. The orange dashed box highlights the section of the ArF with positive ΔCFS .

LI ET AL. 9 of 13



Acknowledgments

We sincerely thank Editor Germán Prieto

and the two anonymous reviewers for their

insightful comments, which have greatly contributed to improving this manuscript. This work was supported by King Abdullah University of Science and

Technology (KAUST, Grants BAS/1/

1339-01-01 and RGC/3/6036-01). TU and AAG acknowledge additional support

from Horizon Europe (ChEESE-2P, Grant

101093038, DT-GEO, Grant 101058129,

and Geo-INQUIRE, Grant 101058518),

the National Aeronautics and Space Administration (80NSSC20K0495), the

National Science Foundation (Grants EAR-2225286, EAR-2121568, OAC-

2139536, OAC-2311208, OAC-2311206)

and the Statewide California Earthquake

gratefully acknowledge the KAUST Supercomputing Laboratory (https://www.

hpc.kaust.edu.sa/) for providing computing resources on the Shaheen II in

Center (SCEC awards 22135, 23121). We

projects k1587 and k1589, and Shaheen III

in project K10043, the Gauss Centre for Supercomputing e.V. (www.gauss-centre.

eu) for providing us with computing time on the supercomputer SuperMUC-NG at

the Leibniz Supercomputing Centre (www.

lrz.de) in projects pr63qo, pn49ha and the

Institute of Geophysics of LMU Munich

(Oeser et al., 2006).

5. Conclusions

This study investigates the 1995 $M_{\rm w}$ 7.2 Nuweiba earthquake through back-projection analysis and dynamic rupture simulations, unraveling a multi-segment cascading rupture that included a supershear rupture on the central Aragonese Fault. While limited resolution prevents detailed analysis of the final rupture phase, backprojection results from multiple global arrays, testing several hypocenter locations, effectively constrain the initiation phase of this debated event, suggesting that the rupture originated on the northern Arnona Fault. Dataconstrained dynamic simulations successfully reproduce the multi-segment cascading rupture, with synthetics demonstrating good alignment with moment rate functions from previous studies and observed teleseismic waveforms. The simulations capture the occurrence of a supershear rupture on the optimally prestressed Aragonese Fault, in agreement with the back-projection observations and surface-wave analysis of Rayleigh waves. The occurrence of such a supershear rupture significantly amplifies seismic hazard in the coastal communities of the narrow gulf, concentrating energy within the Mach cone and resulting in prolonged, intensified ground shaking. The 1995 earthquake only partially ruptured the Gulf of Aqaba fault system, increasing Coulomb failure stress on most of the unbroken Arnona Fault, which likely has remained dormant since 1588. This stress accumulation could accelerate a future rupture on this vulnerable segment, with the potential for a supershear rupture significantly amplifying the seismic hazard in nearby coastal communities, including the rapidly developing NEOM area.

Conflict of Interest

The authors declare no conflicts of interest relevant to this study.

Data Availability Statement

The seismic data used for back-projection and supershear validation is downloaded from the Incorporated Research Institutions for Seismology (IRIS, https://ds.iris.edu/wilber3/find_stations/460922). The topography and bathymetry data is from GeoMapApp (www.geomapapp.org)/(Ryan et al., 2009). The Southern California Earthquake Center(SCEC) Community Benchmark TPV24, from which we adopt the proposed nucleation procedure, is documented in https://strike.scec.org/cvws/tpv24_25docs.html. The dynamic rupture is simulated using the open-source software package SeisSol (https://www.seissol.org), which is freely available from https://github.com/SeisSol/SeisSol. Input files required to reproduce the dynamic simulation can be downloaded from 10.5281/zenodo.15532993 (B. Li & Mai, 2025). The synthetic teleseismic waveform is computed using the IRIS Synthetics Engine (https://ds.iris.edu/ds/products/syngine/), with the 2-s anisotropic PREM model.

References

Abdelazim, M., ElGabry, M. N., Gobashy, M. M., Khalil, M. H., & Hussein, H. M. (2023). Seismicity and fault interaction in the Gulf of Aqaba. Pure and Applied Geophysics, 180(6), 2045–2066. https://doi.org/10.1007/s00024-023-03279-x

Abdel-Fattah, A. K., Hussein, H., & El-Hady, S. (2006). Another look at the 1993 and 1995 Gulf of Aqaba earthquakes from the analysis of teleseismic waveforms. *Acta Geophysica*, 54(3), 260–279. https://doi.org/10.2478/s11600-006-0020-0

Al-shijbi, Y., El-Hussain, I., Deif, A., Al-Kalbani, A., & Mohamed, A. M. (2019). Probabilistic seismic hazard assessment for the Arabian Peninsula. *Pure and Applied Geophysics*, 176(4), 1503–1530. https://doi.org/10.1007/s00024-018-2033-4

Andrews, D. (2010). Ground motion hazard from supershear rupture. Tectonophysics, 493(3-4), 216-221. https://doi.org/10.1016/j.tecto.2010.

Baer, G., Funning, G. J., Shamir, G., & Wright, T. J. (2008). The 1995 November 22, Mw 7.2 Gulf of Elat earthquake cycle revisited. *Geophysical Journal International*, 175(3), 1040–1054. https://doi.org/10.1111/j.1365-246x.2008.03901.x

Bao, H., Ampuero, J.-P., Meng, L., Fielding, E. J., Liang, C., Milliner, C. W., et al. (2019). Early and persistent supershear rupture of the 2018 magnitude 7.5 Palu earthquake. *Nature Geoscience*, 12(3), 200–205. https://doi.org/10.1038/s41561-018-0297-z

Barjous, M., & Mikbel, S. (1990). Tectonic evolution of the Gulf of Aqaba-Dead Sea transform fault system. *Tectonophysics*, 180(1), 49–59. https://doi.org/10.1016/0040-1951(90)90371-e

Bektaş, Z., Avşar, U., Ribot, M., Klinger, Y., & Jónsson, S. (2024). Seismo-turbidites reveal locations of major earthquakes during the past millennium in the Gulf of Aqaba, southern Dead Sea Fault. Earth and Planetary Science Letters, 629, 118595. https://doi.org/10.1016/j.epsl. 2024.118595

Ben-Avraham, Z. (1985). Structural framework of the Gulf of Elat (Aqaba), northern Red Sea. *Journal of Geophysical Research*, 90(B1), 703–726. https://doi.org/10.1029/jb090ib01p00703

Ben-Avraham, Z., Garfunkel, Z., Almagor, G., & Hall, J. K. (1979). Continental breakup by a leaky transform: The Gulf of Elat (Aqaba). Science, 206(4415), 214–216. https://doi.org/10.1126/science.206.4415.214

Bosworth, W., Taviani, M., & Rasul, N. M. (2019). Neotectonics of the Red Sea, Gulf of Suez and Gulf of Aqaba. Geological setting, palae-oenvironment and archaeology of the Red Sea (pp. 11–35).

Bouchon, M., & Karabulut, H. (2008). The aftershock signature of supershear earthquakes. *Science*, 320(5881), 1323–1325. https://doi.org/10.1126/science.1155030

LI ET AL. 10 of 13



Geophysical Research Letters

- 10.1029/2025GL117448
- Castro-Perdomo, N., Viltres, R., Masson, F., Klinger, Y., Liu, S., Dhahry, M., et al. (2022). Interseismic deformation in the Gulf of Aqaba from GPS measurements. *Geophysical Journal International*. 228(1), 477–492, https://doi.org/10.1093/gii/ggab353
- Choi, J.-H., Klinger, Y., Ferry, M., Ritz, J.-F., Kurtz, R., Rizza, M., et al. (2018). Geologic inheritance and earthquake rupture processes: The 1905 M 8 Tsetserleg-Bulnay strike-slip earthquake sequence, Mongolia. *Journal of Geophysical Research: Solid Earth*, 123(2), 1925–1953. https://doi.org/10.1002/2017jb013962
- Corchete, V., Chourak, M., & Hussein, H. (2007). Shear wave velocity structure of the Sinai Peninsula from Rayleigh wave analysis. Surveys in Geophysics, 28(4), 299–324. https://doi.org/10.1007/s10712-007-9027-6
- Daggett, P. H., Morgan, P., Boulos, F., Hennin, S., El-Sherif, A., El-Sayed, A., et al. (1986). Seismicity and active tectonics of the Egyptian Red Sea margin and the northern Red Sea. *Tectonophysics*, 125(4), 313–324. https://doi.org/10.1016/0040-1951(86)90168-x
- Duan, B., & Oglesby, D. D. (2005). Multicycle dynamics of nonplanar strike-slip faults. *Journal of Geophysical Research*, 110(B3), B03304. https://doi.org/10.1029/2004jb003298
- Duan, B., & Oglesby, D. D. (2007). Nonuniform prestress from prior earthquakes and the effect on dynamics of branched fault systems. *Journal of Geophysical Research*, 112(B5), B05308. https://doi.org/10.1029/2006jb004443
- Dunham, E. M., & Bhat, H. S. (2008). Attenuation of radiated ground motion and stresses from three-dimensional supershear ruptures. *Journal of Geophysical Research*, 113(B8), B08319. https://doi.org/10.1029/2007jb005182
- Elhadidy, M., Abdalzaher, M. S., & Gaber, H. (2021). Up-to-date PSHA along the Gulf of Aqaba-Dead Sea transform fault. *Soil Dynamics and Earthquake Engineering*, 148, 106835. https://doi.org/10.1016/j.soildyn.2021.106835
- Eyal, M., Eyal, Y., Bartov, Y., & Steinitz, G. (1981). The tectonic development of the western margin of the Gulf of Elat (Aqaba) rift. *Tecto-*
- nophysics, 80(1–4), 39–66. https://doi.org/10.1016/0040-1951(81)90141-4

 Fang, Z., & Dunham, E. M. (2013). Additional shear resistance from fault roughness and stress levels on geometrically complex faults. *Journal of Geophysical Research: Solid Earth*, 118(7), 3642–3654. https://doi.org/10.1002/jgrb.50262
- Fliss, S., Bhat, H. S., Dmowska, R., & Rice, J. R. (2005). Fault branching and rupture directivity. *Journal of Geophysical Research*, 110(B6), B06312. https://doi.org/10.1029/2004jb003368
- Gabriel, A.-A., Ulrich, T., Marchandon, M., Biemiller, J., & Rekoske, J. (2023). 3D dynamic rupture modeling of the 6 February 2023, Kahramanmaraş, Turkey Mw 7.8 and 7.7 earthquake doublet using early observations. *The Seismic Record*, 3(4), 342–356. https://doi.org/10.1785/
- Galvez, P., Somerville, P., Petukhin, A., Ampuero, J.-P., & Peter, D. (2020). Earthquake cycle modelling of multi-segmented faults: Dynamic rupture and ground motion simulation of the 1992 Mw 7.3 Landers earthquake. *Pure and Applied Geophysics*, 177(5), 2163–2179. https://doi.org/10.1007/s00024-019-02228-x
- Ginzburg, A., Makris, J., Fuchs, K., & Prodehl, C. (1981). The structure of the crust and upper mantle in the Dead Sea rift. *Tectonophysics*, 80(1–4), 109–119. https://doi.org/10.1016/0040-1951(81)90144-x
- Güvercin, S. E., Karabulut, H., Konca, A. Ö., Doğan, U., & Ergintav, S. (2022). Active seismotectonics of the East Anatolian Fault. *Geophysical Journal International*, 230(1), 50–69. https://doi.org/10.1093/gji/ggac045
- Hamouda, A., & El-Gharabawy, S. (2019). Evaluation of the crustal features of the Gulf of Aqaba deduced from geophysical data. *Journal of Geoscience and Environment Protection*, 7(4), 26–41. https://doi.org/10.4236/gep.2019.74003
- Hofstetter, A. (2003). Seismic observations of the 22/11/1995 Gulf of Aqaba earthquake sequence. Tectonophysics, 369(1–2), 21–36. https://doi.org/10.1016/s0040-1951(03)00129-x
- Hofstetter, A., Thio, H., & Shamir, G. (2003). Source mechanism of the 22/11/1995 Gulf of Aqaba earthquake and its aftershock sequence. Journal of Seismology, 7(1), 99–114. https://doi.org/10.1023/a:1021206930730
- Ishii, M., Shearer, P. M., Houston, H., & Vidale, J. E. (2005). Extent, duration and speed of the 2004 Sumatra–Andaman earthquake imaged by the Hi-Net array. *Nature*, 435(7044), 933–936. https://doi.org/10.1038/nature03675
- Ishii, M., Shearer, P. M., Houston, H., & Vidale, J. E. (2007). Teleseismic P wave imaging of the 26 December 2004 Sumatra-Andaman and 28 March 2005 Sumatra earthquake ruptures using the Hi-net array. *Journal of Geophysical Research*, 112(B11), B11307. https://doi.org/10.1029/2006jb004700
- Kaneko, Y., Avouac, J.-P., & Lapusta, N. (2010). Towards inferring earthquake patterns from geodetic observations of interseismic coupling. Nature Geoscience, 3(5), 363–369. https://doi.org/10.1038/ngeo843
- Klinger, Y., Okubo, K., Vallage, A., Champenois, J., Delorme, A., Rougier, E., et al. (2018). Earthquake damage patterns resolve complex rupture processes. Geophysical Research Letters. 45(19), 10–279. https://doi.org/10.1029/2018g1078842
- Klinger, Y., Rivera, L., Haessler, H., & Maurin, J.-C. (1999). Active faulting in the Gulf of Aqaba: New knowledge from the Mw 7.3 earthquake of 22 November 1995. Bulletin of the Seismological Society of America. 89(4), 1025–1036. https://doi.org/10.1785/bssa0890041025
- Koc, A., & Kaymakcı, N. (2013). Kinematics of Sürgü fault zone (Malatya, Turkey): A remote sensing study. *Journal of Geodynamics*, 65, 292–307. https://doi.org/10.1016/j.jog.2012.08.001
- Krüger, F., & Ohrnberger, M. (2005). Tracking the rupture of the M w= 9.3 Sumatra earthquake over 1,150 km at teleseismic distance. *Nature*, 435(7044), 937–939. https://doi.org/10.1038/nature03696
- Li, B., Gabriel, A.-A., & Hillers, G. (2024). Source properties of the pnduced ML 0.0–1.8 earthquakes from local beamforming and backprojection in the Helsinki area, southern Finland. Seismological Research Letters.
- Li, B., Gabriel, A.-A., Ulrich, T., Abril, C., & Halldorsson, B. (2023). Dynamic rupture models, fault interaction and ground motion simulations for the segmented Húsavík-Flatey fault zone, northern Iceland. *Journal of Geophysical Research: Solid Earth*, 128(6), e2022JB025886. https://doi.org/10.1029/2022jb025886
- Li, B., & Ghosh, A. (2017). Imaging rupture process of the 2015 Mw 8.3 Illapel earthquake using the US Seismic Array. In *The Chile-2015* (*Illapel*) earthquake and tsunami (pp. 33–43). Springer.
- Li, B., & Mai, P. M. (2025). Modeling input files for "Supershear rupture of the 1995 Mw 7.2 multi-segment Nuweiba earthquake in the Gulf of Aqaba" [Dataset]. Zenodo. https://doi.org/10.5281/zenodo.15532994
- Li, B., Palgunadi, K. H., Wu, B., Suhendi, C., Zhou, Y., Ghosh, A., & Mai, P. M. (2025). Rupture dynamics and velocity structure effects on ground motion during the 2023 Türkiye earthquake doublet. Communications Earth & Environment, 6(1), 228. https://doi.org/10.1038/s43247-025-02205-4
- Li, X., Jónsson, S., & Cao, Y. (2021). Interseismic deformation from sentinel-1 burst-overlap interferometry: Application to the southern Dead Sea fault. *Geophysical Research Letters*, 48(16), e2021GL093481. https://doi.org/10.1029/2021gl093481
- Lyberis, N. (1988). Tectonic evolution of the Gulf of Suez and the Gulf of Aqaba. Tectonophysics, 153(1-4), 209-220. https://doi.org/10.1016/0040-1951(88)90016-9
- Mahmoud, S., Reilinger, R., McClusky, S., Vernant, P., & Tealeb, A. (2005). GPS evidence for northward motion of the Sinai Block: Implications for E. Mediterranean tectonics. *Earth and Planetary Science Letters*, 238(1–2), 217–224. https://doi.org/10.1016/j.epsl.2005.06.063

LI ET AL. 11 of 13

- Mai, P. M., Aspiotis, T., Aquib, T. A., Cano, E. V., Castro-Cruz, D., Espindola-Carmona, A., et al. (2023). The destructive earthquake doublet of 6 February 2023 in South-Central Türkiye and northwestern Syria: Initial observations and analyses. *The Seismic Record*, 3(2), 105–115. https://doi.org/10.1785/0320230007
- Mai, P. M., Galis, M., Thingbaijam, K. K., Vyas, J. C., & Dunham, E. M. (2018). Accounting for fault roughness in pseudo-dynamic ground-motion simulations. In Best practices in physics-based fault rupture models for seismic hazard assessment of nuclear installations (pp. 95–126).
- Mai, P. M., Li, B., Jonsson, S., Suhendi, C., Liu, J., Li, D., et al. (2025). Breaching a seismic gap: The 2025 magnitude 7.7 Myanmar earthquake. Mogren, S. (2021). Geo-hazard assessment of the NEOM area, Northwest Saudi Arabia, using seismological and potential field data. Arabian Journal of Geosciences, 14(2), 127. https://doi.org/10.1007/s12517-021-06456-1
- Oeser, J., Bunge, H.-P., & Mohr, M. (2006). Cluster design in the earth sciences Tethys. In *International Conference on High Performance Computing and Communications* (pp. 31–40).
- Pinar, A., & Türkelli, N. (1997). Source inversion of the 1993 and 1995 Gulf of Aqaba earthquakes. *Tectonophysics*, 283(1–4), 279–288. https://doi.org/10.1016/s0040-1951(97)00070-x
- Power, W. L., & Tullis, T. E. (1991). Euclidean and fractal models for the description of rock surface roughness. *Journal of Geophysical Research*, 96(B1), 415–424. https://doi.org/10.1029/90jb02107
- Ribot, M., Klinger, Y., Jónsson, S., Avsar, U., Pons-Branchu, E., Matrau, R., & Mallon, F. L. (2021). Active faults' geometry in the Gulf of Aqaba, southern Dead Sea Fault, illuminated by multibeam bathymetric data. *Tectonics*, 40(4), e2020TC006443. https://doi.org/10.1029/2020tc006443
- Ryan, W. B., Carbotte, S. M., Coplan, J. O., O'Hara, S., Melkonian, A., Arko, R., et al. (2009). Global multi-resolution topography synthesis. *Geochemistry, Geophysics, Geosystems*, 10(3), Q03014. https://doi.org/10.1029/2008gc002332
- Shamir, G., Baer, G., & Hofstetter, A. (2003). Three-dimensional elastic earthquake modelling based on integrated seismological and InSAR data: The Mw= 7.2 Nuweiba earthquake, Gulf of Elat/Aqaba 1995 November. *Geophysical Journal International*, 154(3), 731–744. https://doi.org/10.1046/j.1365-246x.2003.01978.x
- Tang, Z., Julià, J., Zahran, H., & Mai, P. M. (2016). The lithospheric shear-wave velocity structure of Saudi Arabia: Young volcanism in an old shield. *Tectonophysics*, 680, 8–27, https://doi.org/10.1016/j.tecto.2016.05.004
- Taufiqurrahman, T., Gabriel, A.-A., Li, D., Ulrich, T., Li, B., Carena, S., et al. (2023). Dynamics, interactions and delays of the 2019 Ridgecrest rupture sequence. *Nature*, 618(7964), 1–8. https://doi.org/10.1038/s41586-023-05985-x
- Ulrich, T., Gabriel, A.-A., Ampuero, J.-P., & Xu, W. (2019). Dynamic viability of the 2016 Mw 7.8 Kaikōura earthquake cascade on weak crustal faults. Natura Communications, 10(1), 1, 16
- faults. Nature Communications, 10(1), 1–16.
 Ulrich, T., Gabriel, A.-A., & Madden, E. H. (2022). Stress, rigidity and sediment strength control megathrust earthquake and tsunami dynamics.
- Nature Geoscience, 15(1), 67–73. https://doi.org/10.1038/s41561-021-00863-5
 Ulrich, T., Vater, S., Madden, E. H., Behrens, J., van Dinther, Y., Van Zelst, I., et al. (2019). Coupled, physics-based modeling reveals earthquake
- displacements are critical to the 2018 Palu, Sulawesi tsunami. *Pure and Applied Geophysics*, 176(10), 4069–4109.
- Vallée, M., Charléty, J., Ferreira, A. M., Delouis, B., & Vergoz, J. (2011). SCARDEC: A new technique for the rapid determination of seismic moment magnitude, focal mechanism and source time functions for large earthquakes using body-wave deconvolution. *Geophysical Journal International*, 184(1), 338–358. https://doi.org/10.1111/j.1365-246x.2010.04836.x
- Vallée, M., & Dunham, E. M. (2012). Observation of far-field Mach waves generated by the 2001 Kokoxili supershear earthquake. *Geophysical Research Letters*, 39(5), L05311. https://doi.org/10.1029/2011gl050725
- Vasyura-Bathke, H., Steinberg, A., Krüger, F., Feng, G., Mai, P. M., & Jónsson, S. (2024). Discontinuous transtensional rupture during the Mw 7.2 1995 Gulf of Aqaba earthquake. Seismica, 3(1). https://doi.org/10.26443/seismica.v3i1.1135
- Vyas, J. C., Mai, P. M., Galis, M., Dunham, E. M., & Imperatori, W. (2018). Mach wave properties in the presence of source and medium heterogeneity. Geophysical Journal International, 214(3), 2035–2052. https://doi.org/10.1093/gji/ggy219
- Wen, Y.-Y., Ma, K.-F., Song, T.-R. A., & Mooney, W. D. (2009). Validation of the rupture properties of the 2001 Kunlun, China (M s= 8.1), earthquake from seismological and geological observations. *Geophysical Journal International*, 177(2), 555–570. https://doi.org/10.1111/j. 1365-246x.2008.04063.x
- Wirp, S. A., Gabriel, A.-A., Ulrich, T., & Lorito, S. (2024). Dynamic rupture modeling of large earthquake scenarios at the Hellenic Arc toward physics-based seismic and tsunami hazard assessment. *Journal of Geophysical Research: Solid Earth*, 129(11), e2024JB029320. https://doi.org/10.1029/2024jb029320
- Wollherr, S., Gabriel, A.-A., & Mai, P. M. (2019). Landers 1992 "reloaded": Integrative dynamic earthquake rupture modeling. *Journal of Geophysical Research: Solid Earth*, 124(7), 6666–6702. https://doi.org/10.1029/2018jb016355
- Wollherr, S., Gabriel, A.-A., & Uphoff, C. (2018). Off-fault plasticity in three-dimensional dynamic rupture simulations using a modal Discontinuous Galerkin method on unstructured meshes: Implementation, verification and application. *Geophysical Journal International*, 214(3), 1556–1584. https://doi.org/10.1093/gji/ggy213
- Xin, D., & Zhang, Z. (2021). On the comparison of seismic ground motion simulated by physics-based dynamic rupture and predicted by empirical attenuation equations. *Bulletin of the Seismological Society of America*, 111(5), 2595–2616. https://doi.org/10.1785/0120210077
- Yilmaz, H., Over, S., & Ozden, S. (2006). Kinematics of the east anatolian fault zone between Turkoglu (Kahramanmaras) and Celikhan (Adiyaman), Eastern Turkey. Earth Planets and Space, 58(11), 1463–1473. https://doi.org/10.1186/bf03352645
- Zhang, L., Zhou, Y., Zhang, X., Zhu, A., Li, B., Wang, S., et al. (2023). 2022 Mw 6.6 Luding, China, earthquake: A strong continental event illuminating the Moxi seismic gap. Seismological Research Letters, 94(5), 2129–2142. https://doi.org/10.1785/0220220383

References From the Supporting Information

- Andrews, D. (1976). Rupture velocity of plane strain shear cracks. *Journal of Geophysical Research*, 81(32), 5679–5687. https://doi.org/10.1029/ib081i032p05679
- Breuer, A., & Heinecke, A. (2022). Next-generation local time stepping for the ADER-DG finite element method. In 2022 IEEE International Parallel and Distributed Processing Symposium (IPDPS) (pp. 402–413).
- Harris, R. A. (1998). Introduction to special section: Stress triggers, stress shadows, and implications for seismic hazard. *Journal of Geophysical Research*, 103(B10), 24347–24358. https://doi.org/10.1029/98jb01576
- Harris, R. A., Barall, M., Aagaard, B., Ma, S., Roten, D., Olsen, K., et al. (2018). A suite of exercises for verifying dynamic earthquake rupture codes. Seismological Research Letters, 89(3), 1146–1162. https://doi.org/10.1785/0220170222

LI ET AL. 12 of 13

- Harris, R. A., Barall, M., Archuleta, R., Dunham, E., Aagaard, B., Ampuero, J. P., et al. (2009). The SCEC/USGS dynamic earthquake rupture code verification exercise. Seismological Research Letters, 80(1), 119–126. https://doi.org/10.1785/gssrl.80.1.119
- Harzali, M., Medhioub, E., Troudi, H., & Bouaziz, S. (2021). The Aqaba Earthquake, 22 November 1995 (7.3 Mw): Insights on the seismicity and active faulting of Gulf of Aqaba. *Arabian Journal of Geosciences*, 14(18), 1915. https://doi.org/10.1007/s12517-021-08252-3
- King, G., & Cocco, M. (2001). Fault interaction by elastic stress changes: New clues from earthquake sequences. In Advances in geophysics (Vol. 44, pp. 1–VIII). Elsevier. https://doi.org/10.1016/s0065-2687(00)80006-0
- King, G. C., Stein, R. S., & Lin, J. (1994). Static stress changes and the triggering of earthquakes. *Bulletin of the Seismological Society of America*, 84(3), 935–953.
- Pelties, C., Gabriel, A.-A., & Ampuero, J.-P. (2014). Verification of an ADER-DG method for complex dynamic rupture problems. *Geoscientific Model Development*, 7(3), 847–866. https://doi.org/10.5194/gmd-7-847-2014
- Roten, D., Olsen, K., Day, S., Cui, Y., & Fäh, D. (2014). Expected seismic shaking in Los Angeles reduced by San Andreas fault zone plasticity. Geophysical Research Letters, 41(8), 2769–2777. https://doi.org/10.1002/2014gl059411
- Suhendi, C., Li, B., Vasyura-Bathke, H., Liu, J., Jónsson, S., & Mai, P. M. (2024). Bayesian inversion and quantitative comparison for bilaterally quasi-symmetric rupture processes on a multi-segment fault in the 2021 Mw 7.4 Maduo earthquake. *Geophysical Journal International*, ggae398.
- Toda, S., Lin, J., & Stein, R. S. (2011). Using the 2011 Mw 9.0 off the Pacific coast of Tohoku Earthquake to test the Coulomb stress triggering hypothesis and to calculate faults brought closer to failure. Earth Planets and Space, 63(7), 725–730. https://doi.org/10.5047/eps.2011.05.010
- Tong, H., Wang, J., Zhao, H., Li, B., Hao, H., & Wang, M. (2014). Mohr space and its application to the activation prediction of pre-existing weakness. *Science China Earth Sciences*, 57(7), 1595–1604. https://doi.org/10.1007/s11430-014-4860-1

LI ET AL. 13 of 13